Delft University of Technology

Impact of MOF defects on the binary adsorption of CO_2 and water in UiO-66

Hossain, Mohammad I.; Cunningham, Jackson D.; Becker, Tim M.; Grabicka, Bogna E.; Walton, Krista S.; Rabideau, Brooks D.; Glover, T. Grant

DOI
10.1016/j.ces.2019.03.053

Publication date
2019

Document Version
Final published version

Published in
Chemical Engineering Science

Citation (APA)
Hossain, M. I., Cunningham, J. D., Becker, T. M., Grabicka, B. E., Walton, K. S., Rabideau, B. D., & Glover, T. G. (2019). Impact of MOF defects on the binary adsorption of CO_2 and water in UiO-66. *Chemical Engineering Science*, *203*, 346-357. https://doi.org/10.1016/j.ces.2019.03.053

Important note
To cite this publication, please use the final published version (if applicable).
Please check the document version above.

Copyright
Other than for strictly personal use, it is not permitted to download, forward or distribute the text or part of it, without the consent of the author(s) and/or copyright holder(s), unless the work is under an open content license such as Creative Commons.

Takedown policy
Please contact us and provide details if you believe this document breaches copyrights.
We will remove access to the work immediately and investigate your claim.

This work is downloaded from Delft University of Technology.
For technical reasons the number of authors shown on this cover page is limited to a maximum of 10.

Chemical Engineering Science 203 (2019) 346–357

Contents lists available at ScienceDirect

Chemical Engineering Science

journal homepage: www.elsevier.com/locate/ces

Impact of MOF defects on the binary adsorption of CO_2 and water in UiO-66

Mohammad I. Hossain [a], Jackson D. Cunningham [a], Tim M. Becker [b], Bogna E. Grabicka [c], Krista S. Walton [c], Brooks D. Rabideau [a], T. Grant Glover [a,*]

[a] University of South Alabama, United States
[b] Delft University of Technology, the Netherlands
[c] Georgia Institute of Technology, United States

HIGHLIGHTS

- Defect sites can have a greater influence on low-pressure CO_2 adsorption in MOFs than the co-adsorption of water.
- CO_2 and H_2O adsorption on UiO-66 MOF occurs non-ideally.
- Molecular simulations accurately capture trends observed in experimentally measured CO_2/H_2O binary adsorption isotherms.

GRAPHICAL ABSTRACT

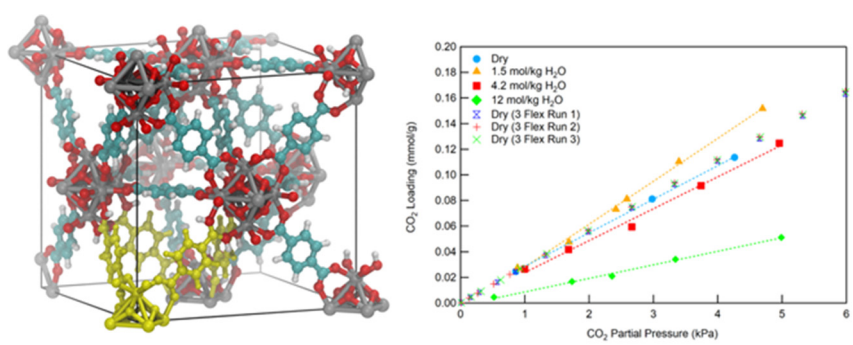

Binary CO_2/H_2O Adsorption on a MOF with Defects

ARTICLE INFO

Article history:
Received 16 November 2018
Received in revised form 11 March 2019
Accepted 23 March 2019
Available online 25 March 2019

Keywords:
MOF
Co-adsorption
CO_2
Defect sites

ABSTRACT

Metal organic frameworks are frequently examined as potential solutions to complex gas phase separations problems. In many cases, the gas phase adsorption properties of these materials are quantified using single component gas adsorption isotherms and breakthrough experiments. In adsorption separations, however, it is common that the adsorbent participates in a multicomponent adsorption event. In the literature there is a general absence of multicomponent adsorption data with most data predicted via the Ideal Adsorbed Solution Theory or molecular simulations. Therefore, in this work, binary adsorption data of CO_2 and water on UiO-66 were measured experimentally using a volumetric method at three different water loadings. Molecular simulations of isotherms were compared to the experimental measurements and the impact of two different MOF defect sites on the multicomponent CO_2/H_2O adsorption behavior was determined. The experimental data show a slight enhancement of CO_2 loading when CO_2 is co-adsorbed with water, which is a result that was confirmed via molecular simulations. Also, the simulation results show that defect sites can have a greater influence on low-pressure CO_2 adsorption in MOFs than the co-adsorption of water. Furthermore, the simulations provide a molecular-level understanding of the role of these defects on the single and binary adsorption behavior.

© 2019 Elsevier Ltd. All rights reserved.

* Corresponding author.
E-mail address: glover@southalabama.edu (T.G. Glover).

https://doi.org/10.1016/j.ces.2019.03.053
0009-2509/© 2019 Elsevier Ltd. All rights reserved.

1. Introduction

Metal organic frameworks (MOFs) are being developed to solve problems in many areas including sensors, separations, catalysis, gas storage, toxic gas filtration, space exploration, CO_2 sequestration, flue gas cleanup, and others (Britt et al., 2009; David Farrusseng, 2011; DeCoste and Peterson, 2014; Doonan et al., 2010; Getman et al., 2012a, 2012b; Glover and Mu, 2018; Glover et al., 2011; Gustafson and Wilmer, 2017; Kaskel, 2016; McDonald et al., 2015, 2012; Scott Bobbitt et al., 2017; Sumida et al., 2012; A. O. Yazaydın et al., 2009). One particular MOF, UiO-66 (Zr 6 (OH) 4O 4 (BDC) 6, BDC = benzene-1,4-dicarboxylate) with hexanuclear Zr_6 inorganic cornerstones has been considered as a candidate for practical applications due to its high stability, resistivity under harsh conditions, tunable properties and high surface area (Bambalaza et al., 2018; Bunge et al., 2018; Hossain et al., 2019; Hu et al., 2017; Shearer et al., 2016; Wu et al., 2013; Yang et al., 2013; Zou and Liu, 2019). In many cases, these applications are seeking to utilize MOFs in multicomponent adsorption situations; however, very little experimental, multicomponent-adsorption data exists in the literature.

In the absence of simple experimental techniques to measure multicomponent isotherm adsorption data, research groups have utilized the Ideal Adsorbed Solution Theory (IAST) to predict multicomponent isotherm data (Cessford et al., 2012; Geier et al., 2013; Jorge et al., 2010; Thompson et al., 2013; Van Assche et al., 2014; Walton and Sholl, 2015; Zhang et al., 2013b, 2013a). Details on IAST are available elsewhere (Myers, 2005; Myers and Prausnitz, 1965; Talu, 1998; Valenzuela and Myers, 1989; Yang, 1997). Briefly, IAST is a thermodynamic approach that assumes an ideal solution is formed by the adsorbed phase. It is an adsorption analog to Raoult's law for vapor-liquid equilibrium, and to meet the ideal requirements, the partial pressure of an adsorbed component is given by the product of its mole fraction in the adsorbed phase and the pressure which it would exert as a pure adsorbed component at the same temperature and spreading pressure as those of the mixture (Myers and Prausnitz, 1965). IAST has limitations in the accuracy of predicted multicomponent isotherm data, and in general, does not capture proper behavior for mixtures of polar species or for mixtures in which one component is strongly adsorbed. Heterogeneity of the adsorbent can also cause poor predictions (Walton and Sholl, 2015). Studies have shown IAST to be highly accurate when applied to ideal adsorbate/adsorbent systems (Chen and Sholl, 2007). Likewise, consistent with the basis of the ideal derivation of IAST, when polar compounds are examined, estimates of selectivities can be incorrect by many orders of magnitude (Bai et al., 2012). It has been shown that IAST is less accurate for MOFs where deviations result from both mixture effects in the form of non-idealities in the adsorbed phase and where the MOF structure has heterogeneities both on the scale of the unit cell and on shorter length scales where competition for the adsorbed site influences the results (Cessford et al., 2012).

In a review of the broad application of IAST to predict multicomponent adsorption behavior, Walton and Sholl highlight that the difficulty of measuring mixed gas adsorption has resulted in few systematic studies that would allow for an evaluation of the accuracy of IAST over a wide range of mixtures, compositions, adsorbents, and conditions (Walton and Sholl, 2015). Similarly, the lack of multicomponent data and the subsequent impact on gas separation processes was emphasized several years ago by Sircar (Sircar, 2006). In this work Sircar states that there is a "desperate need" to understand multicomponent adsorption data and to test existing models. Much like IAST, the general absence of multicomponent adsorption data has broad impacts in the field of molecular simulations because the absence of data prevents the verification of simulations results and subsequent adjustments to force fields and other parameters to capture experimental observations.

Although many works have reported the impact of multicomponent adsorption events in the form of breakthrough and similar separations data (Benoit et al., 2018; Burtch et al., 2014; Chanut et al., 2017; Glover and Mu, 2018; Glover et al., 2011; Llewellyn et al., 2006; Tan et al., 2015); only limited multicomponent adsorption isotherm data for MOFs have been presented in the literature. To our knowledge, the literature has only six papers that report multicomponent adsorption equilibrium for MOFs and of these only three of these papers examine water co-adsorption (Liu et al., 2010; Mason et al., 2015; Ortiz et al., 2012; Hamon et al., 2009, 2012; A. Ö. Yazaydın et al., 2009).

Specifically, LeVan reported CO_2/H_2O binary adsorption isotherms for Cu-BTC and Ni-MOF-74; however, it was later determined that both of these MOFs have only limited stability to water (Burtch et al., 2014). Hamon et al. completed both experimental and theoretical analysis of the binary adsorption of CO_2 and CH_4 on MIL-100 and observed that the predicted selectivities from IAST differ due to the existence of unsaturated accessible metal sites, which interact preferentially with CO_2. However, a modified form of IAST (RAST) improved the theoretical prediction (Hamon et al., 2012). The authors, emphasized the necessity of collecting multicomponent adsorption measurements to accurately evaluate the separation performances of MOFs instead of performing predictions based on single gas adsorption isotherms. Mason et al. has examined multicomponent adsorption data when evaluating MOFs for CO_2/CH_4 separations as well as for post combustion CO_2 capture. In these works, a collection of multicomponent adsorption data points were compared to single component adsorption isotherms to determine the impact of water co-adsorption. Mason et al. discusses the importance of such data and examined CO_2, N_2, and H_2O adsorption on 15 different materials, including MOFs, and noted the degradation of CO_2 adsorption capacity in the presence of water. The authors of this paper also emphasized the lack of experimental data in the literature even though most applications of novel MOF materials will include multiple components (Mason et al., 2015). Lastly, Yazaydin et al. completed a molecular simulation of CO_2/H_2O co-adsorption in Cu-BTC and observed an interaction between the quadrupole moment of CO_2 and the electric field created by the water molecules leading to enhanced CO_2 uptake (A. Ö. Yazaydın et al., 2009). Although these works present some insight on the isotherm, absent from these works are the measurement of CO_2/H_2O binary adsorption isotherms, comparisons of experimental data to models and predictions, and examination of how defects impact CO_2/H_2O adsorption behavior.

Therefore, the purpose of this work is to provide a systematic measurement of the binary gas adsorption isotherms of water and CO_2 covering a range of water loading on a broadly relevant, water stable, MOF and to compare these results to the predicted binary adsorption isotherms using IAST calculations and GCMC simulations. The work will focus on binary CO_2/H_2O adsorption at low CO_2 pressure (below 5 kPa) and molecular simulations examining how the CO_2 and H_2O interact with the MOF in presence of different defect sites in the framework, prior to the framework being completely filled with molecules. Additionally, molecular simulations will be used to examine the binary adsorption behavior up to CO_2 pressures of 1600 kPa.

2. Experimental

2.1. MOF synthesis

Binderless pellets of UiO-66 MOF ($Zr_6O_6(BDC)_6$) were synthesized using methods detailed elsewhere (Jasuja, 2014; Jasuja

et al., 2013). The synthesized powder was then pressed into pellets using a single-punch tablet press machine resulting in pellets having an approximate diameter, thickness and weight of 6 mm, 2 mm and 50 mg respectively. The BET surface area of the pellets was 1059 m^2/g and powder X-ray diffraction patterns are shown in the Supporting Information.

2.2. Multicomponent isotherm measurements

A volumetric system, similar to those detailed by LeVan et al. and detailed in Fig. 1, was constructed (Liu et al., 2010; Rudisill et al., 1992). The volumetric measurements are based on a mass balance principle, which requires characterization of the experimental apparatus volumes. With all the volumes of the system known, a reduction in system pressure was attributed to adsorption and, by monitoring the gas phase composition, the amount of each species in the gas phase that adsorbs was determined via a mass balance. Prior to the measurement, the loop volume, total empty volume and the empty bed volume was determined using He expansion experiment against a calibrated cylinder with known volume. The adsorption bed was filled with a known amount of adsorbent. The bed was regenerated at 150 °C for 12 hrs while pulling vacuum (10^{-4} torr). Then the void volume was determined by He expansion. A pump was installed in line with the system to allow for recirculation of the gas phase to reduce the equilibration time. Three manometers were used with varying full-scale capabilities and each of the manometers were accurate up to 0.01% of full scale and 0.5% of the value indicated. Approximately 2 g of adsorbent were used for the measurement, which was measured on a balance with an accuracy of 0.1 mg up to 220 g. An environmental chamber with a temperature range of −42 °C to 132 °C was used to control temperature. The equilibration time varied between 4 and 48 h depending on the experimental conditions. An Agilent 7890 gas chromatograph (GC) with an Agilent Plot column and a thermal conductivity detector (TCD) was used to separate the adsorbates and identify gas phase concentrations. The linear GC calibration curves had R^2 values of 0.994 and 0.998 for water and CO_2 respectively. The GC was calibrated using a known volume and National Institute of Standards and Technology (NIST) traceable, heated, capacitance-manometers from MKS Instruments, Inc.

2.3. Single component adsorption isotherms

Single component water adsorption isotherms were measured using a Micromeritics ASAP 2020 using approximately 100 mg of MOF. The samples were regenerated on the analysis port for 12 hrs, under vacuum, at 150 °C. Regeneration was completed on the analysis port to ensure that the low-pressure range of the adsorption isotherms was not impacted by atmospheric gases that may enter the cell if it is moved from a regeneration station to the analysis port. Even though a manufacture seal is available for the samples cell, even small amounts of gas have been shown to influence the adsorption isotherms at low pressure (Huang et al., 2017).

Single component CO_2 adsorption isotherms were also measured using the multicomponent volumetric adsorption system discussed above. The samples were regenerated at 150 °C with a low-pressure helium purge overnight. Single component CO_2 adsorption isotherms were also measured using a Micromeritics 3Flex with regeneration taking place on an outgassing instrument at 150 °C overnight and again on the analysis port of the instrument at 150 °C for 3 h.

2.4. Molecular simulations

Three MOF structures of UiO-66 were obtained as crystallographic information files (CIFs) from the Supporting Information of Ghosh et al. (2014) Two of the structures contained single defects in the form of a missing linker, each at a different position as shown in Fig. 5, and one structure was the ideal UiO-66 crystal. These files included the partial charge distribution in the defective MOFs that were rigorously recalculated with DFT calculations in VASP and fitted using the REPEAT method (Campañá et al.,

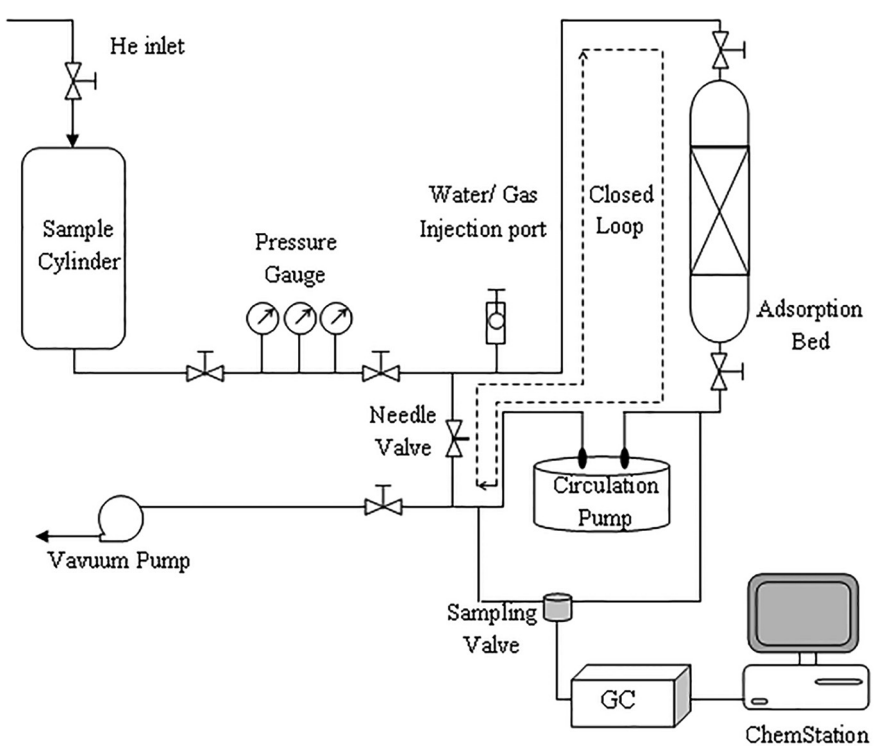

Fig. 1. A block flow diagram of the volumetric adsorption system. Reproduced with permission from ACS Liu et al. (2010).

2009). One would expect a real MOF to have an array of different defect types. Since the scope of the computational study is limited, two different defect types were chosen as "representative" to gauge their effect on adsorption.

As in the original publication, the Lennard-Jones parameters of the zirconium atoms were taken from UFF (Rappe et al., 1992), and the Lennard-Jones parameters of all other atoms were taken from DREIDING (Mayo et al., 1990). The TIP4P model (Jorgensen et al., 1983) was used for water while CO_2 was modeled using the TraPPE force field (Potoff and Siepmann, 2001).

Grand Canonical Monte Carlo (GCMC) simulations were performed with RASPA (version 2) (Dubbeldam et al., 2016). Each roughly cubic MOF structure was replicated one time in each lattice direction. Initially, water was adsorbed into the MOF structure at a temperature of 25 °C and pressures ranging from 0.2 kPa to 4 kPa, each in independent simulations. As noted in the original publication, the uptake of water is a very slow process (Ghosh et al., 2014). Simulations were run on the order of 10^8 simulation cycles, which for some of the simulations, took on the order of weeks to complete. A "cycle" is max(20,N)-move attempts, where N is the number of adsorbed molecules In the case of the ideal MOF structure, no water entered the structure. To accelerate the computation, the GCMC simulations were run with the aid of an energy grid with a refinement of 0.1 nm. A cutoff of 1.2 nm was used for both the short-range dispersion and electrostatic interactions and long-range electrostatics were treated using the Ewald summation technique with a precision of 10^{-6}. The void fraction was determined by probing the framework with a helium molecule using the Widom particle insertion method.

Once the three MOF structures were equilibrated with water, the loadings were fixed, and the combined structures exposed to partial pressures of CO_2. The chemical potentials of water and CO_2 in the mixture were determined using the Peng-Robinson equation of state. Single component isotherms were then determined at 25 °C between 0.2 kPa and 16 MPa in sequential simulations, using the same simulation conditions as before. BET surface areas were calculated for each of the MOF structures and are reported in the Supporting Information. In each case, sequential loading experiments were carried out with N_2 (TraPPE force field) at 77 K.

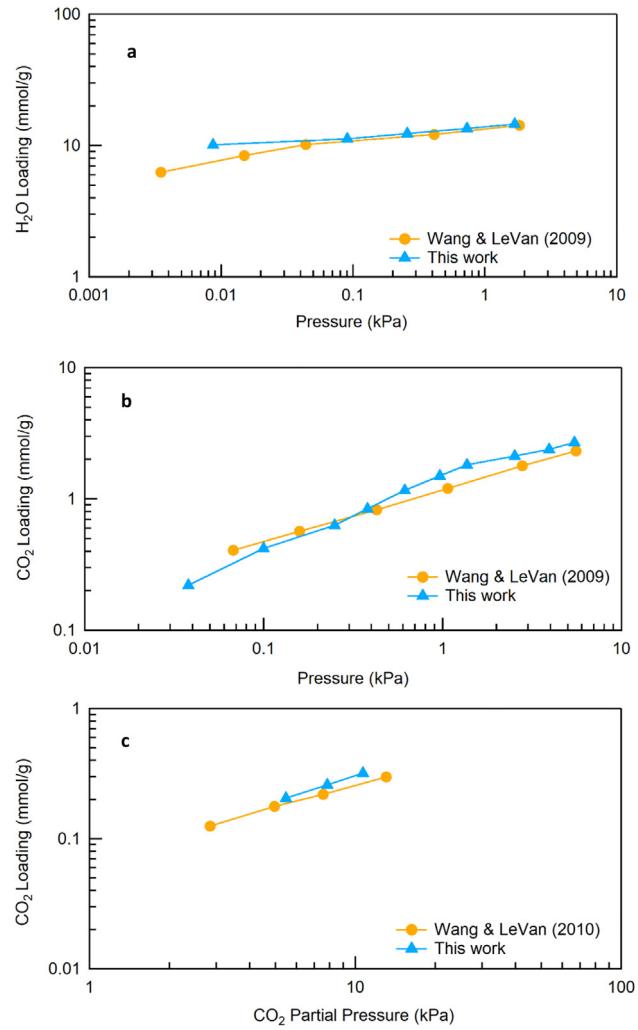

Fig. 2. Single component adsorption isotherm of (a) H_2O and (b) CO_2 on Grace 544 zeolite 13X measured at 25 °C. (c) Binary CO_2/H_2O adsorption isotherms on zeolite 13X at 25 °C. Lines are a guide for the eye.

3. Results and discussion

3.1. Validation of adsorption apparatus – 13X zeolite CO_2/H_2O isotherms

Multicomponent adsorption measurements have been reported for adsorbents other than MOFs with detailed work completed by LeVan (Rudisill et al., 1992; Taqvi et al., 1999; Wang and LeVan, 2010, 2009). It is important to note, that unlike single component adsorption isotherms, binary adsorption isotherms can be reported in different formats depending on the behavior of the adsorbate (Rios et al., 2013). For validation of the adsorption system, H_2O, CO_2, and 13X zeolite were selected as a model system because multicomponent adsorption data for this system have been reported and research has shown that the slope of the adsorption isotherm is particularly sensitive to preadsorbed species making accurate measurement of the CO_2 adsorption capacity challenging (Huang et al., 2017; Wang and LeVan, 2010).

Single component adsorption isotherms measured using the volumetric system are shown in Fig. 2 (and Fig. S1), and the data are consistent with the results of LeVan. The consistency is noteworthy considering that the lot numbers of the 13X zeolite that are measured are likely different (implying different manufacturing batches) even though the same supplier was used (Grace) and that the measurements were independent (measured in two different experimental set-ups by two different individuals). Binary adsorption data was collected by injecting water into the system and equilibrating the water with the adsorbate over time. Next, CO_2 was injected into the system and the system was allowed to equilibrate once again. When water is strongly retained by an adsorbate such that it is not displaced by the co-adsorption of another species, then the multicomponent adsorption data can be plotted as shown in Fig. 2c. In this Figure, CO_2 loading is shown versus CO_2 partial pressure for adsorbents that contain fixed amounts of water adsorbed on the surface of the MOF. This format of binary adsorption data was used previously by LeVan (Wang and LeVan, 2010). The assumption of strongly adsorbed water that is not displaced by a secondary adsorbate, was verified by reading both the water and CO_2 concentrations using the GC at each equilibrium data point and at any intermediate data points that were measured prior to equilibrium. In all cases the adsorbed water was constant throughout the measurement validating this assumption.

While the binary adsorption data also show good agreement with the LeVan data, the LeVan data shown are reported at a constant 9 mol/kg water loading, where the data shown for this work is at a constant 11 mol/kg. The difference of these datasets likely occurs because of a difference in regeneration conditions that were

used. Specifically, the LeVan work cited a regeneration condition of an overnight helium sweep at 200 °C, where the current work employed an overnight evacuation at 350 °C and the pressure was monitored continuously to ensure that by the end of the regeneration period nearly all gases had been removed from the system. After regeneration, and prior to adsorption dosing, the pressure in the system was low enough that a 1 torr transducer was not able to read the system pressure. Additionally, the regeneration took place on the adsorption system (not on a separate device and not transported through the lab and subsequently attached the adsorption device) providing less opportunity for contamination with other adsorbed species. This higher regeneration temperature allows for a more thorough evacuation of water and gives a higher loading of water for the represented behavior. The results shown validate the system as providing accurate single and multicomponent adsorption measurements.

3.2. Experimental UiO-66 CO_2, H_2O, and CO_2/H_2O adsorption isotherms

Single component CO_2 and H_2O adsorption isotherm measured for UiO-66 are shown in Fig. 3. The CO_2 isotherms show a nearly linear adsorption behavior with modest uptake consistent with structure of the MOF having little specific affinity for CO_2. Although the uptake of CO_2 on this MOF is modest, this structure provides a representative baseline Zr MOF to study. Water adsorption isotherms in Fig. 3 show a hydrophobic MOF surface with an S-shaped adsorption isotherm. This type of adsorption isotherm is consistent with other hydrophobic materials, such as water adsorption on BPL activated carbon as well as the behavior that is observed detailing the adsorption of alcohols on ZIFs (Eum et al., 2015).

At low water pressure, the water molecules are adsorbed through H-bonding in two tetrahedral cavities of UiO-66 structure (Canivet et al., 2014). As the water pressure increases, more water molecules are confined in the cavity and hydrogen bond with other adsorbed molecules at the primary binding sites, which leads to the formation of water clusters. Eventually, these secondarily

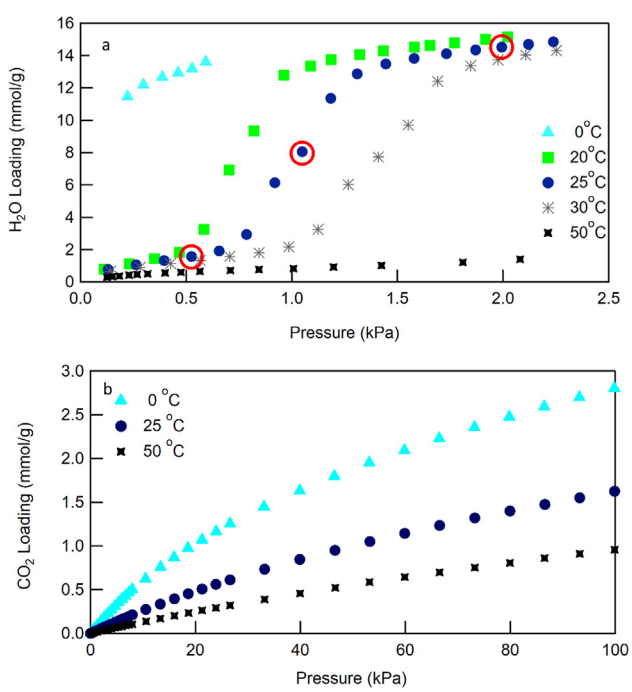

Fig. 3. (a) UiO-66 single component water adsorption isotherms showing the impact of temperature on the inflection point of the isotherm. The circles on the 25 °C adsorption isotherm indicate the points were binary CO_2/H_2O adsorption isotherms where collected. (b) single component adsorption isotherms for CO_2 on UiO-66.

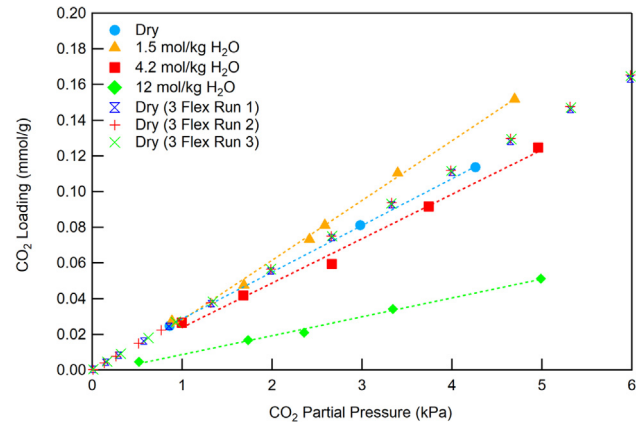

Fig. 4. Binary CO_2/H_2O adsorption isotherms for UiO-66 for three different fixed water loadings. Also shown are single component CO_2 adsorption isotherms for UiO-66 as measured on the volumetric multicomponent system (data shown as circles and labeled "Dry") and compared to single component CO_2 isotherms measured on a commercial instrument (data labeled as "3 Flex Run 1, 2, or 3). The data on both systems are consistent even though the data was collected on different UiO-66 pellets. Lines are a guide for the eye.

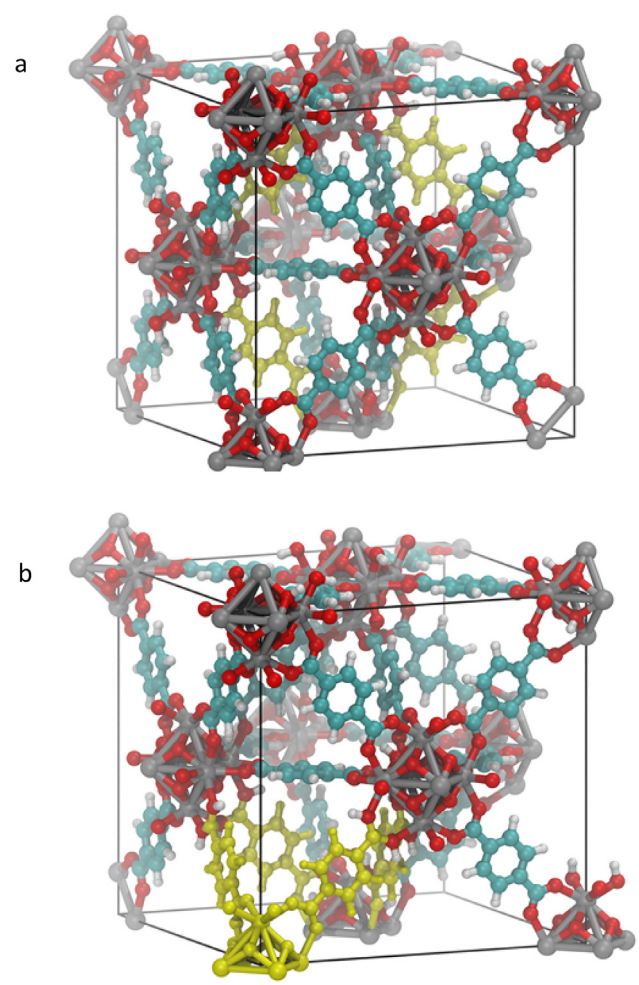

Fig. 5. Molecular structure of UiO-66 with yellow atoms highlighting the areas that were removed to provide defect sites, where oxygen is red, carbon is teal, and hydrogen is white. (a) defect-1 and (b) defect-2. (For interpretation of the references to color in this figure legend, the reader is referred to the web version of this article.)

adsorbed molecules provide further binding sites to facilitate the adsorption in the larger cavities and subsequent water condensation in the framework, which leads to pore filling via a continuous filling process.

The pressure and temperature at which UiO-66 was observed to begin pore filling is consistent with the data of other researchers that also observed that the pore filling occurs at $P/P_o = 0.15–0.3$ (Furukawa et al., 2014; Schoenecker et al., 2012; Wiersum et al., 2011). For comparison the water isotherm of UiO-66 was compared to BPL activated carbon as shown in Fig. S2.(Rudisill et al., 1992) The pore filling occurs first for UiO-66, which has pore sizes of approximately 6 Å followed by BPL carbon, which has a distribution of pore sizes (6–18 Å), which is consistent with the relationship between the adsorption mechanism and pore size.

Both the water and CO_2 isotherms on UiO-66 pellets generally exhibit lower adsorption loading than what has been reported in literature, which can be attributed to the bulk synthesis method and pressing the powder into pellets (Cmarik et al., 2012; Doonan et al., 2010; Jasuja et al., 2012; Peterson et al., 2013). The effect of the large scale synthesis conditions on the adsorption

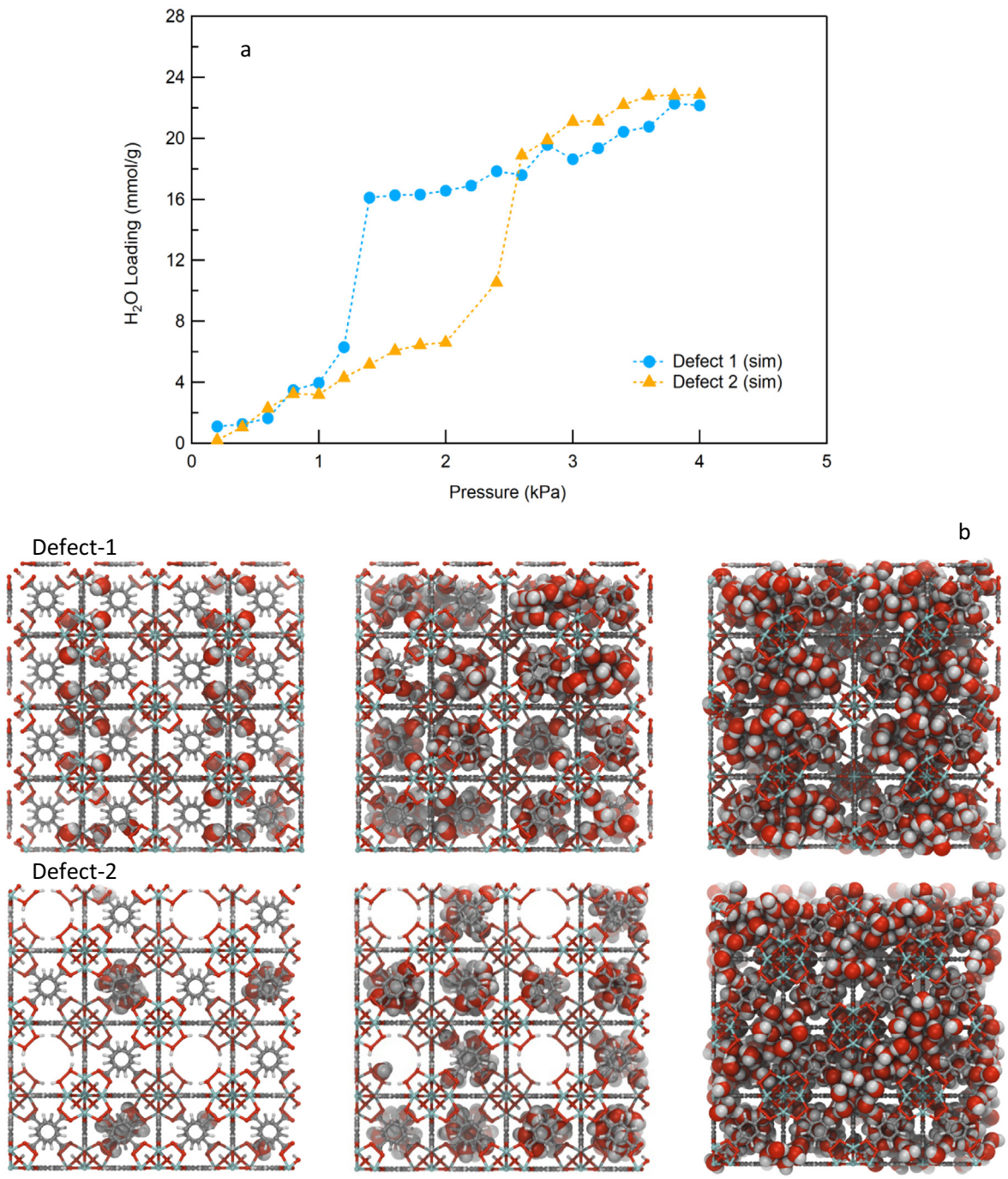

Fig. 6. (a) Water adsorption isotherms for the 2 different defect sites shown in Fig. 5. (b) simulation data showing how water adsorbs in the pores of the MOF. The defects have a significant impact on how the water interacts with the MOF. Defect-1 provides water the opportunity to occupy small spaces near the structural building unit, which changes the amount of water loading at low pressures when compared to defect-2.

properties of UiO-66 have been discussed in detail elsewhere (Jasuja, 2014).

Because of the S-shaped adsorption isotherm binary adsorption measurements were completed at three different locations on the isotherm at 25 °C: at a low water loading (1.5 mol/kg), at the point of pore filling (4.2 mol/kg), and at a point near saturation (12 mol/kg), and each of these points are indicated approximately by a red circle on the water adsorption isotherm shown in Fig. 3. The binary adsorption isotherm data is shown in Fig. 4 for each of the three water loadings for a CO_2 partial pressure from 0 kPa to 5 kPa, and the results are also compared to the single component adsorption data. To further validate the multicomponent adsorption system, single component CO_2 adsorption isotherms were collected on both a Micromeritics 3Flex in triplicate and once on the multicomponent adsorption system and the data was found to be consistent between each system and each measurement as shown in the Fig. 4. Both the water and CO_2 gas phase concentrations were measured using the GC at each equilibrium data point, and at any intermediate data points that were measured prior to equilibrium. The data indicated that water loading was constant, and that water was not displaced with increasing CO_2 concentration.

The results show little reduction from the dry CO_2 adsorption capacity up to at least 4.2 mol/kg, in contrast with reported zeolites. For example, LeVan and Wang state that with 1 mol/kg of adsorbed water the CO_2 capacities decreases more than 30% compared to the pure component adsorption isotherm and by more than 50% when preloaded with 3.4 mol/kg of water (Wang and LeVan, 2010). These data are in contrast to the data collected on the MOF, which shows 7.7% decrease in CO_2 adsorption capacity at 4.2 mol/kg compared to the pure component data.

Surprisingly, the results show a slight increase in the CO_2 adsorption capacity when water is co-adsorbed. The results are consistent with the work of LeVan et al. that showed a slight increase in CO_2 loading when water was pre-adsorbed on Cu-BTC at 25 °C up to 3.4 mol/kg (Liu et al., 2010) and the work of Yazaydin et al. that showed via GCMC simulations that CO_2 loading is enhanced with a 4 wt% water on Cu-BTC MOF at 25 °C (A. Ö. Yazaydın et al., 2009). The simulations of Yazaydin et al. showed the effect was the result of coulombic interactions between the quadrupole moment of CO_2 and the electric field created by H_2O molecules after the introduction of H_2O molecules into the open metal site of MOF structure.

The enhancement of CO_2 adsorption at low pressure in the presence of adsorbed water has also been observed by Rege and Yang in 2001, and Wang and LeVan in 2010 when studying CO_2/H_2O binary adsorption on 13X zeolite (Rege and Yang, 2001; Wang and LeVan, 2010). Rege and Yang state that most cooperative enhancement of adsorption occurs in polar organic compounds that can be attributed to factors, such as hydrogen bonding, but that the increased loading of an inorganic compound such as CO_2 is less straightforward. Similarly, in 1965 it was noted by Bertsch and Habgood that the adsorption rate of CO_2 on zeolite surfaces in the presence of water, with both CO_2 and H_2O at low concentration, was increased (Bertsch and Habgood, 1963). It was proposed that the increased adsorption rate was a result of chemisorption to form a carbonate on the surface. With this in mind, Rege and Yang speculate that it is possible that the increased uptake at low pressure could be attributed to an increase in the adsorption rate in the presence of moisture with some reported zeolite adsorption isotherms being a pseudo-equilibrium since the time of equilibration under a dry conditions is impractically long (Rege and Yang, 2001). This conclusion is consistent with the data of Bertsch and Habgood that the dehydrated zeolite CO_2 adsorption isotherm took more than 60 h to achieve equilibrium at low partial pressure and only minutes when the zeolite was preadsorbed with small amounts of water.

Likewise, in 2010 Wang and LeVan comment that experimental data was not included in figures for low CO_2 partial pressures because the measured loadings were much higher than predictions, which was attributed to chemisorption catalyzed by water leading to the formation of carbonates on the surface. These studies make it clear that CO_2 adsorption on surfaces is complex and may be impacted by chemisorption (carbonate formation). However, it appears that these observations are limited to low pressure isotherms and, in many cases, are not observed at higher adsorp-

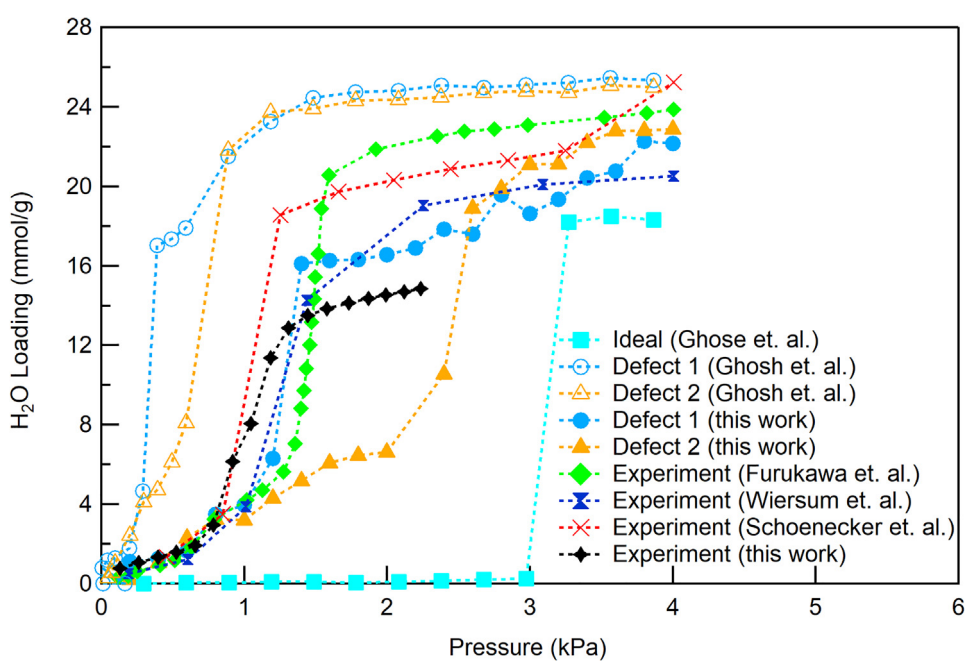

Fig. 7. Water adsorption isotherms as simulated with defect sites 1 and 2 compared to other reported experimental and simulation data in the literature. The exact conditions under which each set of data was collected vary slightly and details are available in the provided references. Lines are a guide for the eye.

tion pressures. To gain additional insight on the adsorption isotherms molecular simulations were completed.

3.3. Computational UiO-66 CO_2, H_2O, and CO_2/H_2O adsorption isotherms

Adsorption isotherms were determined computationally using Grande Canonical Monte Carlo (GCMC) methods, which allows for adsorption data to be collected on both the perfect UiO-66 crystal and UiO-66 containing defects. Studying defects in the context of multicomponent gas adsorption is relevant to this work because the synthesized UiO-66 examined likely has a distribution of different defect sites that are all contributing to the experimentally measured adsorption properties of the material (Sholl and Lively, 2015). Two defect sites were examined by creating two defect unit cells in which each Zr node is missing one linker (out of 12 total), and each missing linker is replaced by 4 hydroxyl groups (2 on each node it was connected to). While the number of defects present in each defect unit cell is identical, the location of these defects differs between the two unit cells as shown in Fig. 5, where atoms in yellow have been removed to provide a defect site in the MOF unit cell.

Representative snapshots of the adsorbed water molecules in defect-1 and 2 at low (1 mol/kg), intermediate (4 mol/kg) and high (22 mol/kg) loadings are also shown in Fig. 6. Here it is readily apparent that water uptake in these MOFs with different types of defects occurs very differently. In defect-1, water adsorbs preferentially on the defect sites at low pressures and is spread out among many individual cavities. As the pressure increases, these defect sites become fully occupied and water begins to fill each individual cavity one by one. At much higher pressures, all of the cavities become filled and the water in each of the cavities interconnect. In contrast to defect-1, water molecules in defect-2 do not adsorb preferentially on the defect sites. Instead, water begins by filling each individual cavity one by one at low pressures. At intermediate pressures, these cells begin to interconnect, and this continues until the structure becomes entirely saturated. Interestingly, such a small change in the location of the defect sites has a huge impact on the shape and behavior of these isotherms.

When the computationally determined single component water adsorption data are compared to other computational water adsorption isotherms in Fig. 7, qualitative agreement is observed. Quantitative differences exist, specifically in the low-pressure water region, which can be attributed to the selection of the critical properties of water. In this work, the critical properties of experimental water were chosen as it provides the best source of comparison with the experimental measurements. Prior studies examining the uptake of water in UIO-66 chose the critical properties of the TIP4P water model (Ghosh et al., 2014). The critical parameters of "real" water were used in the simulation and not the critical parameters of the TIP4P water model. This selection will alter the chemical potential difference between the ideal reservoir and the adsorbed state, which would shift the isotherm. We note here that with a linear rescaling of the x-axis, the two sets of isotherms overlie each other. With defect sites in place, the model isotherm data points follow the experimentally measured data providing confidence in the simulated isotherms.

With confidence that the molecular model is consistent with the works of others, binary adsorption isotherms were simulated for the defect-1 and defect-2 cases at different water loadings (dry, 1.37 mol/kg, and 4.07 mol/kg for defect-1; and dry, 1.08 mol/kg, 4.05 mol/kg for defect-2), as shown in Fig. 8. The data on defect-1 in Fig. 8a, show agreement with the trends observed in the experimental data with an increase in CO_2 loading for 1.37 mol/kg and a decrease at 4.07 mol/kg. The simulation for 12 mol/kg was not completed due to the long computational time

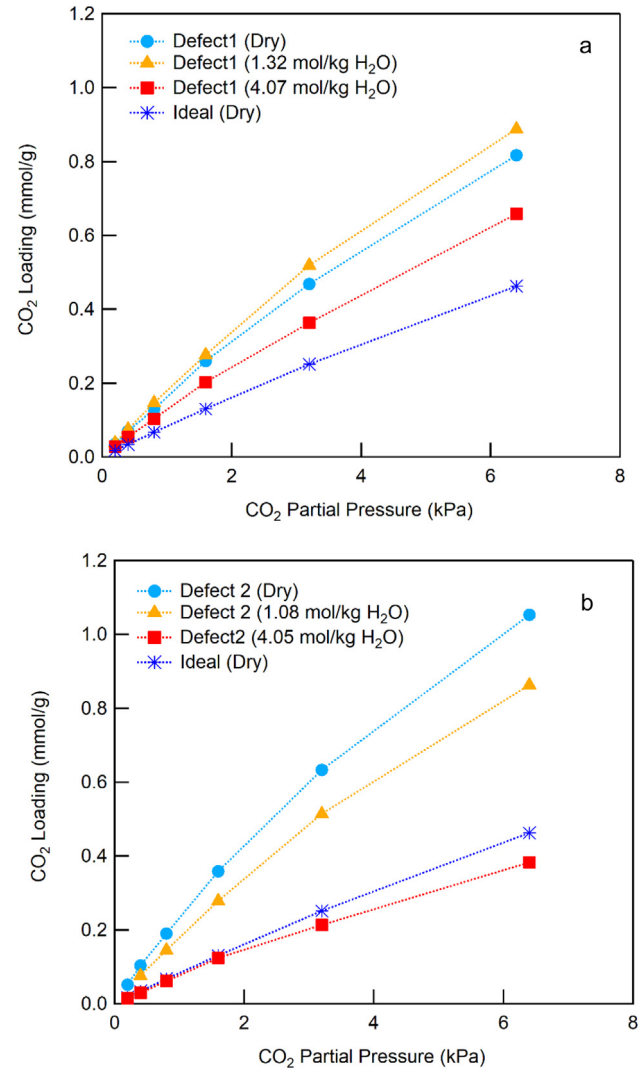

Fig. 8. (a) Binary adsorption isotherms of CO_2/H_2O on UiO-66 for two different MOF defect types. Lines are a guide for the eye.

required to equilibrate the high-water loading and it was concluded that the unique behavior of the binary system had already occurred at lower water loadings. The molecular model is in good agreement with the qualitative trends of the experiments, however the absolute adsorbed amounts of the two differ. This is likely due to the synthesis method used to produce the MOF and its pelletization, which could induce structural defects that differ from the model defects in both number and type.

Specifically, the binary adsorption data measured experimentally and simulated computationally both show interesting non-ideal behavior below 5 kPa. The computational binary adsorption data predict a much higher CO_2 adsorption loading for the given water loadings examined. While there is agreement between the single component experimental data and the simulations data as noted above, when examined closely neither defect-1 or defect-2 models exactly capture the single component adsorption behavior above approximately 0.75 kPa. In particular, the experimental adsorption isotherm data show a greater water loading than either model and a saturation loading that is lower than expected. When examining the work of Ghose et al. the data show that defects produce higher water loadings than perfect crystals. Therefore, it is reasonable that our experimental sample contains either different, or more, defects sites than captured in our model because the water uptake is greater than the model above 0.75 kPa and prior

to saturation. The lower uptake at saturation could be the results of the compression of the adsorbent material to form a pellet, which is also not accounted for in the model.

These differences may provide one possible explanation about why the experimental CO_2 loading in the binary measurement is lower than predicated by the simulation. For example, with a distribution of multiple types, and quantities, of defect sites, the uptake of water at low pressure may be higher, which would result in lower CO_2 loading given the preferential loading of water over CO_2 in this MOF. Additionally, the BET area of the simulated defect-1 and defect-2 MOF structures contained approximately 300 m^2/g more surface area than the experimental pellet (Table S1), which would also result in a higher loading of adsorbates in the simulations. While the quantitative differences are present, the simulations do accurately capture the trends observed in the binary adsorption data and provide a high degree of confidence that the experimentally observed trend is correct.

Moreover, the simulations provide a molecular explanation for this enhanced uptake of CO_2 at low water loadings. In defect-1 at low pressures, water preferentially adsorbs at the defect sites in the corners of each cavity, leaving the volume of each cavity relatively unfilled. When water adsorbs to these sites, it is held relatively fixed with one of the hydrogen atoms directed towards the metal center and the electronegative oxygen atom exposed and directed towards the center of the cavity. This allows CO_2 to enter the center of these cavities with minimal steric repulsion and interact favorably through electrostatic interactions with the adsorbed water molecules as shown in the snapshot of the binary CO_2/H_2O simulation in Fig. 9. As the pressure is increased to intermediate concentrations (a water loading of 4.07 mol/kg), water begins to fill the individual cells, which leads to volume exclusion effects. At the higher water loading fewer CO_2 molecules are able to enter the cells and the enhancement in CO_2 adsorption is not observed.

Defect-2, conversely, shows no enhancement of CO_2 adsorption at low water loadings (Fig. 9), which can be attributed to the very different way in which water adsorbs into the structure. Since water in defect-2 initially loads cell-by-cell instead of preferentially at the defect sites, volume is initially excluded, and CO_2 is unable to adsorb into the same cell as water and benefit from the favorable electrostatic interactions, as shown in Fig. 9.

Regarding the impact of defect sites, when binary CO_2/H_2O simulations were completed on perfect crystals of UiO-66, the simulations struggled to collect any data as a result of the difficulty placing water in the perfect crystal. This was also noted in a prior study with UIO-66, where water uptake in the ideal MOF structure was only observed above the saturation pressure (Ghosh et al., 2014). When the isotherms of the defect-1 and defect-2 are compared to the ideal UiO-66 isotherm, the results show that both defects have a significant impact on the CO_2 capacity. In particular, when considered broadly both defects provide adsorption capacities in a similar range and the adsorbed amount in both cases is higher than the ideal case. Moreover, because the addition of water does not diminish the capacity of the defect laden material until approximately 4 mol/kg of water loading, it can be concluded that

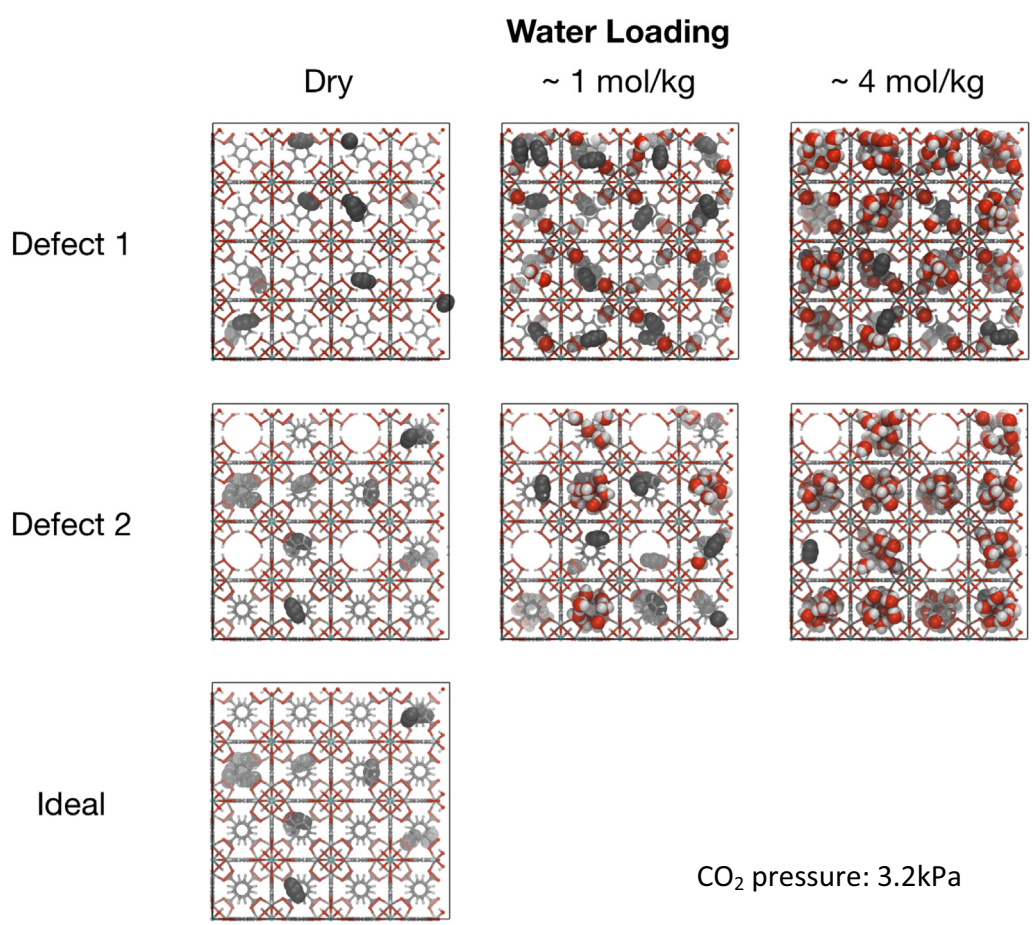

Fig. 9. Molecular simulations showing the location of water and CO_2 in UiO-66 in a binary adsorption event. How the adsorbates fill the MOF is a strong function of the presence, and types, of defects contained in the MOF.

defects have a greater impact on CO_2 loading than the co-adsorption of water until approximately 4 mol/kg of water loading.

The results show that the molecular simulations provide a prediction of the adsorbed phase behavior and capture the unexpected trend of enhanced CO_2 adsorption with the presence of some water. Therefore, because measuring binary adsorption data is time consuming, and with the molecular simulations validated, simulations were used to examine the binary CO_2/H_2O adsorption isotherms up to 11 bar. The results show (Fig. 10) that the defect-1 CO_2/H_2O adsorption isotherm has a CO_2 adsorption capacity below that of the defect-1 dry CO_2 adsorption isotherms for pressures above approximately 15 kPa. The crossing of the defect-1 dry and defect-1 1.32 mol/kg water CO_2 adsorption isotherms is consistent with the filling of the MOF pore space by the CO_2 such that eventually water is simply taking up space in the pore that could be occupied by CO_2.

The ability of GCMC to capture the CO_2 enhancement with co-adsorption of water is interesting because these simulations do not consider reactions. It is possible that similar to zeolites, that water on UiO-66 results in the formation of carbonates, but the molecular simulations are indicating that the CO_2 enhancement can occur by a physical adsorption process too. It is also possible that in the experimental measurement that the physical adsorption enhancement subsequently leads to carbonate formation and that the experimental measurements are reflecting both phenomena. On zeolites, the CO_2 enhancement was found to occur mainly at low CO_2 partial pressures, which is consistent with the MOF data. Because of the tunable nature of MOFs, it is likely that a detailed study of MOF surface functionalization and topology is needed to gather a more detailed understanding of this phenomena.

These results are important because it shows that multicomponent effects can be influenced by the presence of defects and that the adsorbate/adsorbate interactions may be secondary to the adsorbate defect site interactions on the total gas loading. This further emphasizes a need to understand defect sites in MOFs and to design MOFs to utilize these defect sites to impact gas separations.

Lastly, the data were compared to IAST predictions for CO_2/H_2O adsorption on UiO-66 as shown in Fig. 11. A comparison to IAST was completed because, as noted in the introduction, IAST has been used extensively in the literature; however, application of IAST to the CO_2/H_2O system was done with the recognition that CO_2/H_2O likely does not conform to the underlying IAST assumptions, mainly, the formation of an ideal homogenous mixture in the adsorbed phase.

The IAST data were calculated using the full pressure range of the single component experimental adsorption isotherm data. Single component CO_2 adsorption isotherm data was used from the lowest available pressure data for the adsorbate to approximately 101 kPa for CO_2 and then fit with the Langmuir isotherm to estimate the spreading pressure for the IAST calculation (shown in Supporting Information), which is consistent with recommendation by others (Talu, 1998; Walton and Sholl, 2015). Because the water loading has minimal impact on CO_2 loading up to approximately 4 mol/kg, the IAST does well in capturing the binary behavior at 1.4 and 4.2 mol/kg of co-adsorbed water. However, because

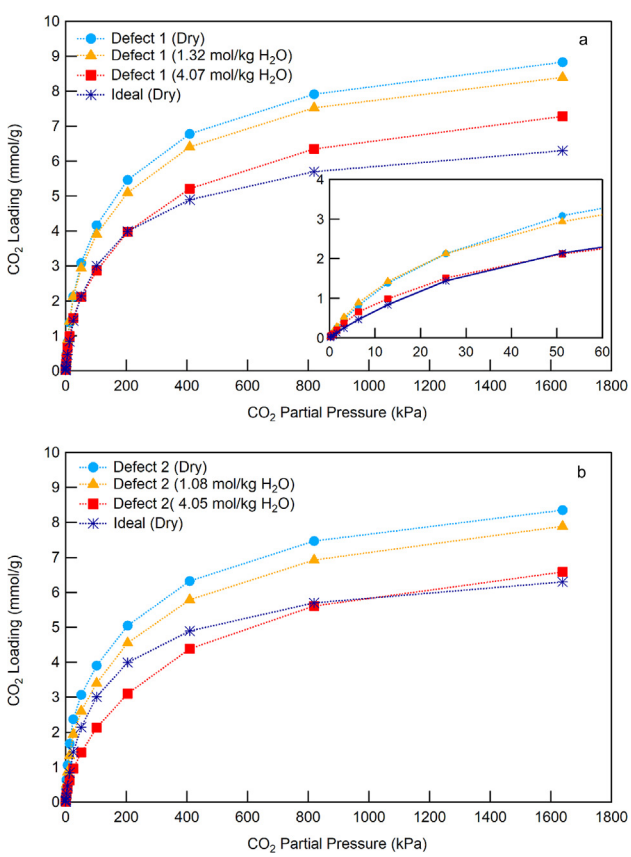

Fig. 10. (a) Binary CO_2/H_2O adsorption isotherms simulations extended to higher pressure highlighting the impact water co-adsorption for UiO-66 containing defects on CO_2 capacity. (b) The defect-1 CO_2 isotherm at 1.32 mol/kg of water crosses the dry defect-1 adsorption isotherm at approximately 15 kPa. Lines are a guide for the eye.

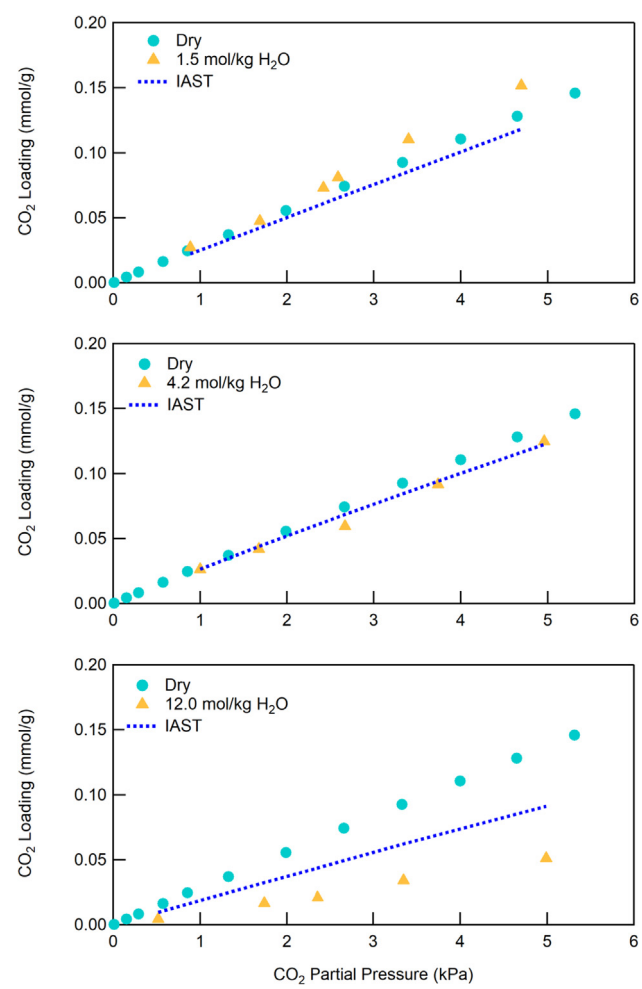

Fig. 11. Experimental binary CO_2/H_2O adsorption isotherms compared to IAST for UiO-66 MOF.

the observed CO_2 enchantment in the binary data occurs because of adsorbent surface specific interaction (non-ideal behavior) or possibly chemisorption (carbonates), the IAST fails to capture the subtle changes in CO_2 adsorption upon co-adsorption with water, as would be expected of an ideal approximation of the binary behavior. By 12 mol/kg the water is competing with the CO_2 for the adsorption surface/space and the IAST fails to capture the competitive behavior.

4. Conclusion

Binary CO_2/H_2O adsorption isotherm data on UiO-66 have been collected and compared to both GCMC and IAST calculations. The results show that defect sites in the MOF have a greater impact on CO_2 loading than water co-adsorption up to water loadings of approximately 4 mol/kg. The molecular simulations show that the mechanism of CO_2 loading changes depending on the type of defect in the MOF structure. An enhancement of CO_2 loading upon co-adsorption of water was also observed in the experimentally-collected binary adsorption isotherms. The enhancement was also seen in the molecular simulations, but only for one defect type indicating that not only are defects important, but the type of defect will also impact gas adsorption isotherms. The molecular simulations accurately capture the trends observed in the experimentally collected co-adsorption isotherms of CO_2 and H_2O providing a high degree of confidence in molecular simulations of multicomponent adsorption isotherms in MOFs. IAST does not capture the subtle changes in the adsorption isotherms and fails to capture the adsorption isotherms at a water loading of 12 mol/kg. However, because the CO_2 loading is not affected by water co-adsorption up to approximately 4 mol/kg, IAST does provide a general indication of the adsorption capacity of the material up to 4 mol/kg of water adsorption. Broadly, the results illustrate the accuracy of GCMC simulations; the need to understand how defect sites in MOFs impact multicomponent adsorption; and show that non-ideal CO_2 behavior is possible even on MOFs with limited surface functionality.

Declaration of interests

The authors declare that they have no known competing financial interests

Acknowledgments

The authors graciously acknowledge financial support from NASA Cooperative Agreement Notice NNH16ZHA001C Experimental Program to Stimulate Competitive Research under contract NNX16AT47A, the Space Grant Foundation NASA X-Hab Program, and the Alabama EPSCoR Graduate Student Fellowship Program.

Appendix A. Supplementary material

Supplementary data to this article can be found online at https://doi.org/10.1016/j.ces.2019.03.053.

References

Bai, P., Tsapatsis, M., Siepmann, J.I., 2012. Multicomponent adsorption of alcohols onto silicalite-1 from aqueous solution: isotherms, structural analysis, and assessment of ideal adsorbed solution theory. Langmuir 28, 15566–15576. https://doi.org/10.1021/la303247c.

Bambalaza, S.E., Langmi, H.W., Mokaya, R., Musyoka, N.M., Ren, J., Khotseng, L.E., 2018. Compaction of a zirconium metal–organic framework (UiO-66) for high density hydrogen storage applications. J. Mater. Chem. A 6, 23569–23577. https://doi.org/10.1039/C8TA09227C.

Benoit, V., Chanut, N., Pillai, R.S., Benzaqui, M., Beurroies, I., Devautour-Vinot, S., Serre, C., Steunou, N., Maurin, G., Llewellyn, P.L., 2018. A promising metal–organic framework (MOF), MIL-96(Al), for CO_2 separation under humid conditions. J. Mater. Chem. A 6, 2081–2090. https://doi.org/10.1039/C7TA09696H.

Bertsch, L., Habgood, H.W., 1963. An infrared spectroscopic study of the adsorption of water and carbon dioxide by linde molecular sieve x1. J. Phys. Chem., 1621–1628

Britt, D., Furukawa, H., Wang, B., Glover, T.G., Yaghi, O.M., 2009. Highly efficient separation of carbon dioxide by a metal-organic framework replete with open metal sites. PNAS 106, 20637–20640. https://doi.org/10.1073/pnas.0909718106.

Bunge, M.A., Davis, A.B., West, K.N., West, C.W., Glover, T.G., 2018. Synthesis and characterization of UiO-66-NH2 metal-organic framework cotton composite textiles. Ind. Eng. Chem. Res. 57, 9151–9161. https://doi.org/10.1021/acs.iecr.8b01010.

Burtch, N.C., Jasuja, H., Walton, K.S., 2014. Water stability and adsorption in metal-organic frameworks. Chem. Rev. 114, 10575–10612. https://doi.org/10.1021/cr5002589.

Campañá, C., Mussard, B., Woo, T.K., 2009. Electrostatic potential derived atomic charges for periodic systems using a modified error functional. J. Chem. Theory Comput. 5, 2866–2878. https://doi.org/10.1021/ct9003405.

Canivet, J., Fateeva, A., Guo, Y., Coasne, B., Farrusseng, D., 2014. Water adsorption in MOFs: fundamentals and applications. Chem. Soc. Rev. 43, 5594–5617. https://doi.org/10.1039/C4CS00078A.

Cessford, N.F., Seaton, N.A., Düren, T., 2012. Evaluation of ideal adsorbed solution theory as a tool for the design of metal-organic framework materials. Ind. Eng. Chem. Res. 51, 4911–4921. https://doi.org/10.1021/ie202219w.

Chanut, N., Bourrelly, S., Kuchta, B., Serre, C., Chang, J.-S., Wright, P.A., Llewellyn, P.L., 2017. Screening the effect of water vapour on gas adsorption performance: application to CO_2 capture from flue gas in metal-organic frameworks. ChemSusChem 10, 1543–1553. https://doi.org/10.1002/cssc.201601816.

Chen, H., Sholl, D.S., 2007. Examining the accuracy of ideal adsorbed solution theory without curve-fitting using transition matrix Monte Carlo simulations. Langmuir 23, 6431–6437. https://doi.org/10.1021/la700351c.

Cmarik, G.E., Kim, M., Cohen, S.M., Walton, K.S., 2012. Tuning the Adsorption Properties of UiO-66 via Ligand Functionalization. Langmuir 28, 15606–15613. https://doi.org/10.1021/la3035352.

Farrusseng, David (Ed.), 2011. Metal-Organic Frameworks: Applications from Catalysis to Gas Storage - David Farrusseng. Wiley-VCH, Weinheim, Germany.

DeCoste, J.B., Peterson, G.W., 2014. Metal-organic frameworks for air purification of toxic chemicals. Chem. Rev. 114, 5695–5727. https://doi.org/10.1021/cr4006473.

Doonan, C.J., Tranchemontagne, D.J., Glover, T.G., Hunt, J.R., Yaghi, O.M., 2010. Exceptional ammonia uptake by a covalent organic framework. Nat. Chem. 2, 235–238. https://doi.org/10.1038/nchem.548.

Dubbeldam, D., Calero, S., Ellis, D.E., Snurr, R.Q., 2016. RASPA: molecular simulation software for adsorption and diffusion in flexible nanoporous materials. Mol. Simul. 42, 81–101. https://doi.org/10.1080/08927022.2015.1010082.

Eum, K., Jayachandrababu, K.C., Rashidi, F., Zhang, K., Leisen, J., Graham, S., Lively, R. P., Chance, R.R., Sholl, D.S., Jones, C.W., Nair, S., 2015. Highly tunable molecular sieving and adsorption properties of mixed-linker zeolitic imidazolate frameworks. J. Am. Chem. Soc. 137, 4191–4197. https://doi.org/10.1021/jacs.5b00803.

Furukawa, H., Gándara, F., Zhang, Y.-B., Jiang, J., Queen, W.L., Hudson, M.R., Yaghi, O. M., 2014. Water adsorption in porous metal-organic frameworks and related materials. J. Am. Chem. Soc. 136, 4369–4381. https://doi.org/10.1021/ja500330a.

Geier, S.J., Mason, J.A., Bloch, E.D., Queen, W.L., Hudson, M.R., Brown, C.M., Long, J.R., 2013. Selective adsorption of ethylene over ethane and propylene over propane in the metal–organic frameworks M2(dobdc) (M = Mg, Mn, Fe Co, Ni, Zn). Chem. Sci. 4, 2054–2061. https://doi.org/10.1039/c3sc00032j.

Getman, R.B., Bae, Y.-S., Wilmer, C.E., Snurr, R.Q., 2012. Review and analysis of molecular simulations of methane, hydrogen, and acetylene storage in metal-organic frameworks. Chem. Rev. 112, 703–723. https://doi.org/10.1021/cr200217c.

Ghosh, P., Colón, Y.J., Snurr, R.Q., 2014a. Water adsorption in UiO-66: the importance of defects. Chem. Commun. 50, 11329–11331. https://doi.org/10.1039/C4CC04945D.

Glover, T.G., Mu, B. (Eds.), 2018. Gas Adsorption in Metal-Organic Frameworks: Fundamentals and Applications. Taylor & Francis.

Glover, T.G., Peterson, G.W., Schindler, B.J., Britt, D., Yaghi, O., 2011. MOF-74 building unit has a direct impact on toxic gas adsorption. Chem. Eng. Sci. 66, 163–170. https://doi.org/10.1016/j.ces.2010.10.002.

Gustafson, J.A., Wilmer, C.E., 2017. Computational design of metal-organic framework arrays for gas sensing: influence of array size and composition on sensor performance. J. Phys. Chem. C 121, 6033–6038. https://doi.org/10.1021/acs.jpcc.6b09740.

Hamon, L., Heymans, N., Llewellyn, P.L., Guillerm, V., Ghoufi, A., Vaesen, S., Maurin, G., Serre, C., De Weireld, G., Pirngruber, G.D., 2012. Separation of CO2–CH4 mixtures in the mesoporous MIL-100(Cr) MOF: experimental and modelling approaches. Dalton Trans. 41, 4052. https://doi.org/10.1039/c2dt12102f.

Hamon, L., Llewellyn, P.L., Devic, T., Ghoufi, A., Clet, G., Guillerm, V., Pirngruber, G.D., Maurin, G., Serre, C., Driver, G., van Beek, W., Jolimaître, E., Vimont, A., Daturi, M., Férey, G., 2009. Co-adsorption and separation of CO_2–CH_4 mixtures in the highly flexible MIL-53(Cr) MOF. J. Am. Chem. Soc. 131, 17490–17499. https://doi.org/10.1021/ja907556q.

Hossain, M.I., Udoh, A., Grabicka, B.E., Walton, K.S., Ritchie, S.M.C., Glover, T.G., 2019. Membrane-coated UiO-66 MOF adsorbents. Ind. Eng. Chem. Res. 58, 1352–1362. https://doi.org/10.1021/acs.iecr.8b05275.

Hu, Z., Wang, Y., Farooq, S., Zhao, D., 2017. A highly stable metal-organic framework with optimum aperture size for CO2 capture. AIChE J. 63, 4103–4114. https://doi.org/10.1002/aic.15837.

Huang, R., Richardson, T.-M.J., Belancik, G., Jan, D., 2017. CO2 capacity sorbent analysis using volumetric measurement approach. Presented at the 47th International Conference on Environmental Systems, Charleston, South Carolina.

Jasuja, H., 2014. Developing Design Criteria and Scale up Methods for Water-stable Metal-organic Frameworks for Adsorption Applications. Georgia Institute of Technology, Atlanta, Georgia, USA.

Jasuja, H., Fletcher, D., Walton, K.S., 2013. Effect of Solvent Reduction on the Synthesis of the Highly Robust Z-BDC (UiO-66) MOF.

Jasuja, H., Zang, J., Sholl, D.S., Walton, K.S., 2012. Rational tuning of water vapor and CO_2 adsorption in highly stable Zr-based MOFs. J. Phys. Chem. C 116, 23526–23532. https://doi.org/10.1021/jp308657x.

Jorge, M., Lamia, N., Rodrigues, A.E., 2010. Molecular simulation of propane/propylene separation on the metal–organic framework CuBTC. Colloids Surf., A 357, 27–34. https://doi.org/10.1016/j.colsurfa.2009.08.025.

Jorgensen, W.L., Chandrasekhar, J., Madura, J.D., Impey, R.W., Klein, M.L., 1983. Comparison of simple potential functions for simulating liquid water. J. Chem. Phys. 79, 926–935. https://doi.org/10.1063/1.445869.

Kaskel, S., 2016. The Chemistry of Metal-Organic Frameworks: Synthesis, Characterization, and Applications, 2 Volumes - Stefan Kaskel. Wiley-VCH Verlag GmbH & Co KGaA.

Liu, J., Wang, Y., Benin, A.I., Jakubczak, P., Willis, R.R., LeVan, M.D., 2010. CO_2/H_2O adsorption equilibrium and rates on metal−organic frameworks: HKUST-1 and Ni/DOBDC. Langmuir 26, 14301–14307. https://doi.org/10.1021/la102359q.

Llewellyn, P.L., Bourrelly, S., Serre, C., Filinchuk, Y., Férey, G., 2006. How hydration drastically improves adsorption selectivity for CO_2 over CH_4 in the flexible chromium terephthalate MIL-53. Angew. Chem. Int. Ed. 45, 7751–7754. https://doi.org/10.1002/anie.200602278.

Mason, J.A., McDonald, T.M., Bae, T.-H., Bachman, J.E., Sumida, K., Dutton, J.J., Kaye, S. S., Long, J.R., 2015. Application of a high-throughput analyzer in evaluating solid adsorbents for post-combustion carbon capture via multicomponent adsorption of CO_2, N_2, and H_2O. J. Am. Chem. Soc. 137, 4787–4803. https://doi.org/10.1021/jacs.5b00838.

Mayo, S.L., Olafson, B.D., Goddard, W.A., 1990. DREIDING: a generic force field for molecular simulations. J. Phys. Chem. 94, 8897–8909.

McDonald, T.M., Lee, W.R., Mason, J.A., Wiers, B.M., Hong, C.S., Long, J.R., 2012. Capture of carbon dioxide from air and flue gas in the alkylamine-appended metal-organic framework mmen-Mg_2 (dobpdc). J. Am. Chem. Soc. 134, 7056–7065. https://doi.org/10.1021/ja300034j.

McDonald, T.M., Mason, J.A., Kong, X., Bloch, E.D., Gygi, D., Dani, A., Crocellà, V., Giordanino, F., Odoh, S.O., Drisdell, W.S., Vlaisavljevich, B., Dzubak, A.L., Poloni, R., Schnell, S.K., Planas, N., Lee, K., Pascal, T., Wan, L.F., Prendergast, D., Neaton, J. B., Smit, B., Kortright, J.B., Gagliardi, L., Bordiga, S., Reimer, J.A., Long, J.R., 2015. Cooperative insertion of CO2 in diamine-appended metal-organic frameworks. Nature 519, 303–308. https://doi.org/10.1038/nature14327.

Myers, A.L., 2005. Prediction of adsorption of nonideal mixtures in nanoporous materials. Adsorption 11, 37–42.

Myers, A.L., Prausnitz, J.M., 1965. Thermodynamics of mixed-gas adsorption. AIChE J. 11, 121–127. https://doi.org/10.1002/aic.690110125.

Ortiz, A.U., Springuel-Huet, M.-A., Coudert, F.-X., Fuchs, A.H., Boutin, A., 2012. Predicting mixture coadsorption in soft porous crystals: experimental and theoretical study of CO_2/CH_4 in MIL-53(Al). Langmuir 28, 494–498. https://doi.org/10.1021/la203925y.

Peterson, G.W., DeCoste, J.B., Glover, T.G., Huang, Y., Jasuja, H., Walton, K.S., 2013. Effects of pelletization pressure on the physical and chemical properties of the metal–organic frameworks Cu3(BTC)2 and UiO-66. Microporous Mesoporous Mater. 179, 48–53. https://doi.org/10.1016/J.MICROMESO.2013.02.025.

Potoff, J.J., Siepmann, J.I., 2001. Vapor–liquid equilibria of mixtures containing alkanes, carbon dioxide, and nitrogen. AIChE J. 47, 1676–1682. https://doi.org/10.1002/aic.690470719.

Rappe, A.K., Casewit, C.J., Colwell, K.S., Goddard, W.A., Skiff, W.M., 1992. UFF, a full periodic table force field for molecular mechanics and molecular dynamics simulations. J. Am. Chem. Soc. 114, 10024–10035. https://doi.org/10.1021/ja00051a040.

Rege, S.U., Yang, R.T., 2001. A novel FTIR method for studying mixed gas adsorption at low concentrations: H_2O and CO_2 on NaX zeolite and γ-alumina. Chem. Eng. Sci. 56, 3781–3796. https://doi.org/10.1016/S0009-2509(01)00095-1.

Rios, R.B., Stragliotto, F.M., Peixoto, H.R., Torres, A.E.B., Bastos-Neto, M., Azevedo, D. C.S., Cavalcante Jr, C.L., 2013. Studies on the adsorption behavior of CO_2-CH_4 mixtures using activated carbon. Braz. J. Chem. Eng. 30, 939–951. https://doi.org/10.1590/S0104-66322013000400024.

Rudisill, E.N., Hacskaylo, J.J., LeVan, M.D., 1992. Coadsorption of hydrocarbons and water on BPL activated carbon. Ind. Eng. Chem. Res. 31, 1122–1130. https://doi.org/10.1021/ie00004a022.

Schoenecker, P.M., Carson, C.G., Jasuja, H., Flemming, C.J.J., Walton, K.S., 2012. Effect of water adsorption on retention of structure and surface area of metal-organic frameworks. Ind. Eng. Chem. Res. 51, 6513–6519. https://doi.org/10.1021/ie202325p.

Scott Bobbitt, N., Mendonca, L., Howarth, M.J., Islamoglu T, A., Hupp, T., Farha, J.K., Snurr R, O.Q., 2017. Metal–organic frameworks for the removal of toxic industrial chemicals and chemical warfare agents. Chem. Soc. Rev. 46, 3357–3385. https://doi.org/10.1039/C7CS00108H.

Shearer, G.C., Chavan, S., Bordiga, S., Svelle, S., Olsbye, U., Lillerud, K.P., 2016. Defect engineering: tuning the porosity and composition of the metal-organic framework UiO-66 via modulated synthesis. Chem. Mater. 28, 3749–3761. https://doi.org/10.1021/acs.chemmater.6b00602.

Sholl, D.S., Lively, R.P., 2015. Defects in metal-organic frameworks: challenge or opportunity? J. Phys. Chem. Lett. 6, 3437–3444. https://doi.org/10.1021/acs.jpclett.5b01135.

Sircar, S., 2006. Basic research needs for design of adsorptive gas separation processes. Ind. Eng. Chem. Res. 45, 5435–5448. https://doi.org/10.1021/ie051056a.

Sumida, K., Rogow, D.L., Mason, J.A., McDonald, T.M., Bloch, E.D., Herm, Z.R., Bae, T.-H., Long, J.R., 2012. Carbon dioxide capture in metal-organic frameworks. Chem. Rev. 112, 724–781. https://doi.org/10.1021/cr2003272.

Talu, O., 1998. Needs, status, techniques and problems with binary gas adsorption experiments. Adv. Colloid Interface Sci. 76–77, 227–269. https://doi.org/10.1016/S0001-8686(98)00048-7.

Tan, K., Zuluaga, S., Gong, Q., Gao, Y., Nijem, N., Li, J., Thonhauser, T., Chabal, Y.J., 2015. Competitive coadsorption of CO_2 with H_2O, NH_3, SO_2, NO, NO_2, N_2, O_2, and CH_4 in M-MOF-74 (M = Mg Co, Ni): the role of hydrogen bonding. Chem. Mater. 27, 2203–2217. https://doi.org/10.1021/acs.chemmater.5b00315.

Taqvi, S.M., Appel, W.S., LeVan, M.D., 1999. Coadsorption of organic compounds and water vapor on BPL activated Carbon. 4. Methanol, ethanol, propanol, butanol, and modeling. Ind. Eng. Chem. Res. 38, 240–250. https://doi.org/10.1021/ie980324k.

Thompson, J.A., Brunelli, N.A., Lively, R.P., Johnson, J.R., Jones, C.W., Nair, S., 2013. Tunable CO $_2$ adsorbents by mixed-linker synthesis and postsynthetic modification of zeolitic imidazolate frameworks. J. Phys. Chem. C 117, 8198–8207. https://doi.org/10.1021/jp312590r.

Valenzuela, D.P., Myers, A.L., 1989. Adsorption Equilibrium Data Handbook. Prentice Hall, Englewood Cliffs, N.J..

Van Assche, T.R.C., Duerinck, T., Van der Perre, S., Baron, G.V., Denayer, J.F.M., 2014. Prediction of molecular separation of polar-apolar mixtures on heterogeneous metal-organic frameworks: HKUST-1. Langmuir 30, 7878–7883. https://doi.org/10.1021/la5020253.

Walton, K.S., Sholl, D.S., 2015. Predicting multicomponent adsorption: 50 years of the ideal adsorbed solution theory. AIChE J. 61, 2757–2762. https://doi.org/10.1002/aic.14878.

Wang, Y., LeVan, M.D., 2010. Adsorption equilibrium of binary mixtures of carbon dioxide and water vapor on zeolites 5A and 13X. J. Chem. Eng. Data 55, 3189–3195. https://doi.org/10.1021/je100053g.

Wang, Y., LeVan, M.D., 2009. Adsorption equilibrium of carbon dioxide and water vapor on zeolites 5A and 13X and silica gel: pure components. J. Chem. Eng. Data 54, 2839–2844. https://doi.org/10.1021/je800900a.

Wiersum, A.D., Soubeyrand-Lenoir, E., Yang, Q., Moulin, B., Guillerm, V., Yahia, M.B., Bourrelly, S., Vimont, A., Miller, S., Vagner, C., Daturi, M., Clet, G., Serre, C., Maurin, G., Llewellyn, P.L., 2011. An Evaluation of UiO-66 for Gas-Based Applications. Chem. Asian J. 6, 3270–3280. https://doi.org/10.1002/asia.201100201.

Wu, H., Yildirim, T., Zhou, W., 2013. Exceptional mechanical stability of highly porous zirconium metal-organic framework UiO-66 and its important implications. J. Phys. Chem. Lett. 4, 925–930. https://doi.org/10.1021/jz4002345.

Yang, Q., Vaesen, S., Ragon, F., Wiersum, A.D., Wu, D., Lago, A., Devic, T., Martineau, C., Taulelle, F., Llewellyn, P.L., Jobic, H., Zhong, C., Serre, C., De Weireld, G., Maurin, G., 2013. A water stable metal-organic framework with optimal features for CO_2 capture. Angew. Chem. Int. Ed. 52, 10316–10320. https://doi.org/10.1002/anie.201302682.

Yang, R.T., 1997. Gas Separation by Adsorption Processes. Imperial College Press, London.

Yazaydın, A.Ö., Benin, A.I., Faheem, S.A., Jakubczak, P., Low, J.J., Willis, R.R., Snurr, R. Q., 2009a. Enhanced CO_2 adsorption in metal-organic frameworks via occupation of open-metal sites by coordinated water molecules. Chem. Mater. 21, 1425–1430. https://doi.org/10.1021/cm900049x.

Yazaydın, A.O., Snurr, R.Q., Park, T.-H., Koh, K., Liu, J., LeVan, M.D., Benin, A.I., Jakubczak, P., Lanuza, M., Galloway, D.B., Low, J.J., Willis, R.R., 2009b. Screening of metal−organic frameworks for carbon dioxide capture from flue gas using a combined experimental and modeling approach. J. Am. Chem. Soc. 131, 18198–18199. https://doi.org/10.1021/ja9057234.

Zhang, K., Lively, R.P., Dose, M.E., Brown, A.J., Zhang, C., Chung, J., Nair, S., Koros, W.J., Chance, R.R., 2013a. Alcohol and water adsorption in zeolitic imidazolate frameworks. Chem. Commun. 49, 3245–3247. https://doi.org/10.1039/c3cc39116g.

Zhang, K., Lively, R.P., Zhang, C., Koros, W.J., Chance, R.R., 2013b. Investigating the intrinsic ethanol/water separation capability of ZIF-8: an adsorption and diffusion study. J. Phys. Chem. C 117, 7214–7225. https://doi.org/10.1021/jp401548b.

Zou, D., Liu, D., 2019. Understanding the modifications and applications of highly stable porous frameworks via UiO-66. Mater. Today Chem. 12, 139–165. https://doi.org/10.1016/j.mtchem.2018.12.004.